AGU PUBLICATIONS

Geochemistry, Geophysics, Geosystems

RESEARCH ARTICLE

10.1002/2016GC006511

Key Points:
- Magnetite growth was observed in 17–100% serpentinized abyssal peridotites from the Yokoniwa Rise in the Central Indian Ridge
- Rock magnetic analyses clearly show nonlinear nature of magnetite contents and magnetization associated with serpentinization
- Interacting single-domain magnetite grains formed during the later stage of serpentinization after formation of superparamagnetic grains

Supporting Information:
- Supporting Information S1

Correspondence to:
M. Fujii,
fujii.masakazu@nipr.ac.jp

Citation:
Fujii, M., K. Okino, H. Sato, K. Nakamura, T. Sato, and T. Yamazaki (2016), Variation in magnetic properties of serpentinized peridotites exposed on the Yokoniwa Rise, Central Indian Ridge: Insights into the role of magnetite in serpentinization, *Geochem. Geophys. Geosyst.*, *17*, 5024–5035, doi:10.1002/2016GC006511.

Received 29 JUN 2016
Accepted 24 NOV 2016
Accepted article online 20 DEC 2016
Published online 27 DEC 2016

Variation in magnetic properties of serpentinized peridotites exposed on the Yokoniwa Rise, Central Indian Ridge: Insights into the role of magnetite in serpentinization

Masakazu Fujii[1], Kyoko Okino[2], Hiroshi Sato[3], Kentaro Nakamura[4], Taichi Sato[5], and Toshitsugu Yamazaki[2]

[1]National Institute of Polar Research/SOKENDAI, Tachikawa, Tokyo, Japan, [2]Atmosphere and Ocean Research Institute, The University of Tokyo, Kashiwa, Chiba, Japan, [3]Senshu University, Tama, Kawasaki, Kanagawa, Japan, [4]The University of Tokyo, Bunkyo, Tokyo, Japan, [5]Geological Survey of Japan, AIST, Tsukuba, Ibaraki, Japan

Abstract Magnetic properties in serpentinized peridotites are of increasing interest in seafloor mapping and petrologic studies because such data can promote the understanding of serpentinization reactions and hydrogen creation in ultramafic rocks. In order to reveal the magnetic properties and magnetite growth in serpentinized peridotites, we analyzed 30 serpentinized peridotite samples from a nontransform offset massif called the Yokoniwa Rise in the Central Indian Ridge. The results from multiple rock magnetic analyses and petrological observations illustrate the details of the creation and growth of magnetite in serpentinized peridotites that have undergone 17–100% serpentinzation. The magnetic carrier of these samples is pure magnetite, which did not suffer from maghemitization (low-temperature oxidation). The magnetic susceptibility ranged from 0.002 to 0.087 SI and increased nonlinearly with the progression of the serpentinization reaction. The natural remanent magnetization intensities of 0.2–8.4 A/m are comparable to those of basalts, which suggests that the remanence as well as induced magnetization of highly serpentinized peridotite can contribute to magnetization of the oceanic lithosphere. The amount of magnetite estimated from saturation magnetization increased nonlinearly from 0.1 to 5.5 wt % with the progression of the serpentinization. Highly serpentinized peridotites have a well-developed serpentine mesh texture. Pseudo-single-domain (PSD) and multidomain (MD) grains were formed during igneous processes in the mantle and/or during the initial stages of serpentinization. Superparamagnetic (SP) particles were formed during the initial stages of serpentinization. Single-domain (SD) magnetite was formed during the later stage of serpentinization, and it is assembled inside of mesh structures with strong magnetostatic interactions.

1. Introduction

Seafloor explorations have revealed that serpentinized peridotites are commonly exposed on the seafloor in slow-spreading environments [e.g., *Dick*, 1989; *Cannat et al.*, 1995; *Michael et al.*, 2003]. The alteration of mantle peridotite into serpentine plays a key role in providing hydrogen to chemosynthetic ecosystems [e.g., *Takai et al.*, 2006] and in the formation of volcanogenic massive sulfide deposits in ultramafic-hosted hydrothermal vent systems [e.g., *Fouquet et al.*, 2010]. Serpentinization changes the physical properties of the oceanic lithosphere, including its density, seismic velocity, rheology, electrical conductivity, and magnetic properties [e.g., *Toft et al.*, 1990; *Dyment et al.*, 1997; *Escartín et al.*, 1997; *Katayama et al.*, 2009]. Sea surface geophysical mapping studies reported enhanced magnetization intensities near nontransform offsets (NTOs) involving oceanic core complex (OCC) terrains at mid-ocean ridges [e.g., *Okino et al.*, 2004]. High-resolution deep-sea magnetic studies have also found strong magnetization intensities at active ultramafic-hosted hydrothermal fields [e.g., *Szitkar et al.*, 2014; *Fujii et al.*, 2016]. These signatures were interpreted as being the result of magnetite creation through serpentinization of ultramafic rocks. However, our knowledge of the natural remanent magnetization and magnetic susceptibility for abyssal peridotites is still limited. Previous work by *Oufi et al.* [2002] investigated the magnetic properties of variably serpentinized abyssal peridotites from seven deep-sea drilling sites, but the serpentinization degree of their samples was limited to 40–100%. In this range, the compiled data show that magnetic susceptibility increases with the progression of serpentinization and some highly serpentinized peridotites have high natural remanent magnetization but show large regional differences, which makes it difficult to understand the nonlinear change of magnetic properties in the serpentinization reaction. Laboratory experiments by *Malvoisin et al*. [2012] demonstrated that the rock magnetic approach is a powerful tool for precise monitoring of serpentinization kinetics and the production of hydrogen that is bound to the magnetite production rate. Investigations of abyssal peridotites recently exposed on the seafloor can provide important constraints for the serpentinization mechanism through comparisons to samples from xenolith [e.g., *Ferré et al*., 2013] and onland OCC [e.g., *Maffione et al*., 2014] because they are expected to have preserved the primary state of geological history without suffering from weathering, low-temperature oxidation, and tectonic metamorphism. In this paper, we report on a comprehensive data set for the magnetic and petrological properties of abyssal peridotites and discuss the magnetite creation and growth in relation to serpentinization processes. The samples we used had a wide range of serpentinization degrees that ranged from 17% to 100%, and these samples were collected from a NTO massif called the Yokoniwa Rise in the Central Indian Ridge (CIR).

2. Geological Background

The Yokoniwa Rise is situated in the southernmost segment, namely CIR-S1, of the CIR near the Rodriguez triple junction (Figure 1). The CIR is a slow-spreading to intermediate-spreading ridge system and is segmented by many fracture zones and NTOs [e.g., *Briais*, 1995]. The CIR-S1 is a 20 km segment with a well-developed axial valley, where volcanic cones without deformation are distributed along a neo-volcanic zone. It was considered that the CIR-S1 was newly created during the evolution of the triple junction since the segment length shortens in the older off-axis area [*Munschy and Schlich*, 1989; *Mendel et al*., 2000]. The spreading axes have a right lateral offset of 26 km between the CIR-S1 and S2. Ridge-parallel abyssal hill patterns are distributed along the trace of this NTO, where several domed highs composed of ultramafic rocks are present, such as the 25°S OCC, Uraniwa Hills, and Phoenix knoll [*Kumagai et al*., 2008; *Morishita et al*., 2009, 2015; *Nakamura et al*., 2009; *Sato et al*., 2009; *Okino et al*., 2015] Between two nodal basins of CIR-S1

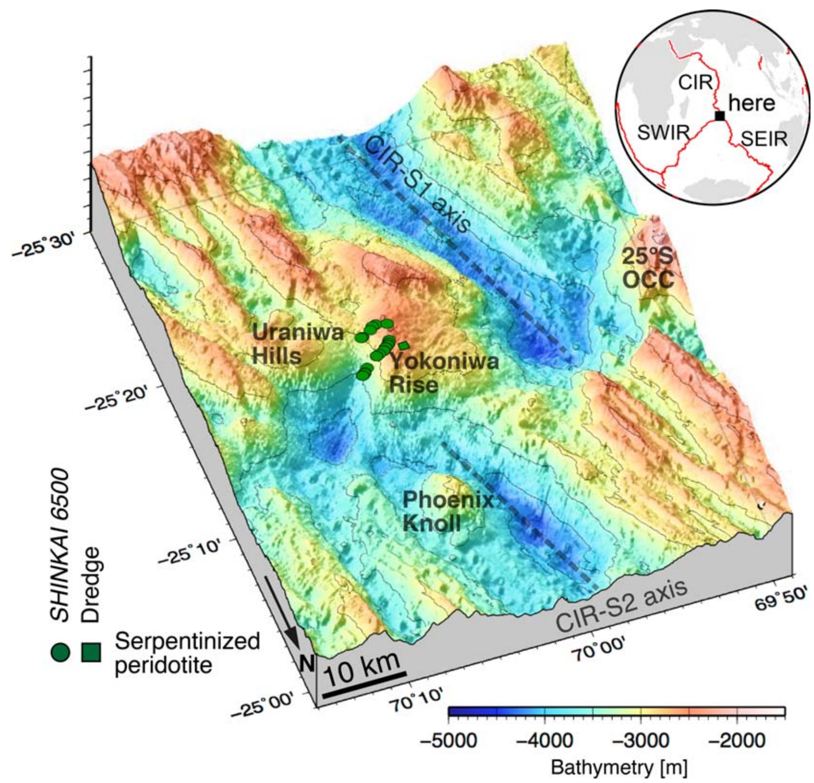

Figure 1. Sample locations illustrated with a seafloor bathymetric map of the Central Indian Ridge (CIR) segments 1 and 2. All samples were collected on a nontransform massif of the Yokoniwa Rise near a nontransform discontinuity. Bathymetry data are from *Okino et al*. [2015]. The circles and the square show sampling done with SHINKAI 6500 dives and a dredge haul, respectively. OCC, oceanic core complex; SWIR, Southwest Indian Ridge; and SEIR, Southeast Indian Ridge.

and CIR-S2, the Yokoniwa Rise occurs with a height of 1700 m from the rift valley floor as shallow dome-like NTO massif [*Okino et al*., 2015; *Fujii et al*., 2016]. Sea-surface magnetic anomalies were identified along the Brunhes/Matuyama boundary in the eastern off-axis area of CIR-S1 and S2 far from the Yokoniwa Rise [*Honsho et al*., 1996; *Sato et al*., 2009; *Okino et al*., 2015]. These results suggest that the Yokoniwa Rise formed during the Brunhes normal chron (<0.78 Ma). An inactive hydrothermal vent field with diminishing low-temperature venting and small dead chimneys was found on top of the Yokoniwa Rise, where enhanced near-seafloor magnetic anomalies were observed by the autonomous underwater vehicle (AUV) *r2D4* at an altitude of 80 m (avg.) [*Fujii et al*., 2016].

3. Materials and Methods

Measurements of rock magnetic properties, density, and petrological observations were performed on 30 serpentinized peridotite samples (Table 1). These samples were collected from the surface of the Yokoniwa Rise at a depth of 2500–3400 m. The sampling was conducted by three dive surveys of the submersible *SHINKAI 6500* during the R/V *Yokosuka* YK09-13-leg2 cruise and by a dredge haul conducted during the R/V *Hakuho-maru* KH10-5 cruise (Figure 1).

The serpentinized peridotites are represented by clinopyroxene-bearing harzburgites to lherzolites. Microstructures were examined on polished thin sections, and back-scattered electron (BSE) images were acquired using a transmitted and reflected light microscopy (Figure 2), a scanning electron microscopy (SEM; Hitachi High-Tech SU3500), and a field emission SEM (Hitachi High-Tech SU 8200). Most samples displayed macroscopic foliation resulting from variable amounts of dynamic recrystallization of olivine grains. Some samples with light brown color had experienced weathering processes. Peridotites with low serpentinzation degrees were characterized by sparse veins developed within or around olivine grains. With

Table 1. Rock Magnetic Properties, Density, and Serpentinization Degree of 30 Serpentinized Peridotites Collected on the Yokoniwa Rise in the Central Indian Ridge

Sample Name	Density (kg/m^3)	NRM (A/m)	K (SI)	Q	Ms (Am^2/kg)	*m* (wt %)	S (%)	MDF (mT)	Latitude (°)	Longitude (°)	Depth (m)
6K#1170R01	2.66	2.5	0.057	1.4	3.5	3.8	94	16	−25.2497	70.1021	3420
6K#1170R03	2.68	3.5	0.060	1.9	2.7	2.9	89	22	−25.2497	70.1021	3420
6K#1170R04	2.72	3.9	0.042	2.9	2.9	3.2	84	29	−25.2496	70.1006	3315
6K#1170R05	2.67	2.2	0.040	1.8	3.2	3.5	92	18	−25.2496	70.1006	3315
6K#1170R08	2.87	2.4	0.024	3.1	1.4	1.5	59	20	−25.2496	70.1003	3298
6K#1170R09	2.70	2.2	0.048	1.5	2.1	2.2	84	21	−25.2516	70.0974	3216
6K#1170R12	2.68	8.4	0.073	3.6	4.4	4.8	96	25	−25.2532	70.0881	2987
6K#1170R14	3.14	0.9	0.012	2.2	0.7	0.7	22	36	−25.2532	70.0881	2987
6K#1170R15	3.08	0.7	0.013	1.8	0.7	0.8	30	21	−25.2526	70.0858	2885
6K#1170R19	3.10	0.9	0.015	1.8	1.2	1.3	29	40	−25.2518	70.0821	2783
6K#1170R20	2.66	2.6	0.047	1.7	2.8	3.0	92	13	−25.2518	70.0821	2783
6K#1170R21	2.71	1.5	0.046	1.0	2.3	2.5	84	18	−25.2521	70.0803	2700
6K#1170R22	2.66	1.3	0.019	2.1	0.8	0.8	85	24	−25.2521	70.0803	2700
6K#1170R23	2.63	3.0	0.021	4.6	1.0	1.1	88	37	−25.2521	70.0803	2700
6K#1170R25	3.17	0.3	0.002	5.7	0.1	0.1	17	44	−25.2524	70.0783	2635
6K#1170R26	3.05	0.6	0.012	1.5	0.3	0.4	33	38	−25.2524	70.0783	2635
6K#1170R27	3.04	1.3	0.025	1.7	0.8	0.9	36	30	−25.2530	70.0772	2569
6K#1170R31	2.82	0.4	0.005	2.9	1.3	1.4	65	47	−25.2542	70.0763	2539
6K#1176R01	2.65	2.5	0.024	3.3	2.6	2.8	93	56	−25.2748	70.0934	3031
6K#1176R03	2.64	6.2	0.069	2.8	4.3	4.7	100	28	−25.2747	70.0924	2998
6K#1176R04	2.73	2.5	0.087	0.9	4.3	4.6	88	24	−25.2747	70.0924	2998
6K#1176R09	2.65	1.9	0.035	1.7	2.8	3.1	93	44	−25.2741	70.0857	2763
6K#1176R10	2.87	1.3	0.027	1.5	1.2	1.3	59	31	−25.2738	70.0838	2657
6K#1176R15	2.65	1.5	0.051	0.9	2.4	2.7	92	34	−25.2730	70.0810	2530
6K#1176R21	2.75	3.9	0.066	1.9	5.0	5.5	89	19	−25.2682	70.0724	2491
DR11-002	2.84	0.2	0.015	0.4	0.3	0.3	60	43	−25.2450	70.0666	2594
DR11-003	2.81	0.8	0.020	1.3	1.5	1.6	67	90	−25.2450	70.0666	2594
DR11-004	2.75	1.0	0.026	1.2	2.5	2.8	79	35	−25.2450	70.0666	2594
DR11-008	2.78	0.4	0.014	0.8	0.9	0.9	69	28	−25.2450	70.0666	2594
DR11-011	2.74	4.4	0.047	2.9	3.9	4.3	85	34	−25.2450	70.0666	2594

Abbreviations are NRM, natural remanent magnetization; K, magnetic susceptibility; Q, Koenigsberger ratio; Ms, saturation magnetization; *m*, magnetite amount; S, serpentinization degree; and MDF, median destructive field.

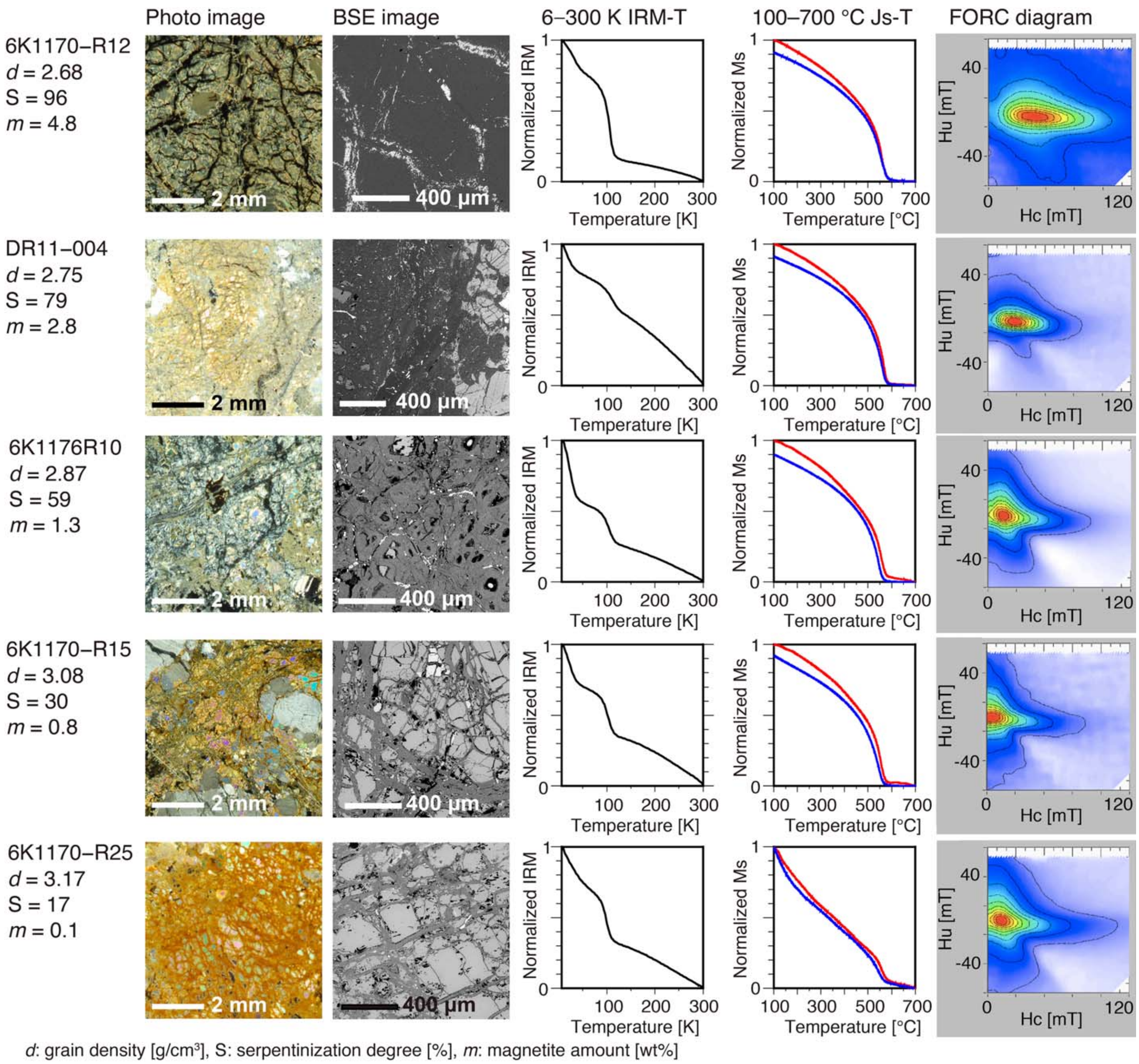

Figure 2. Polarization images, back-scattered electron (BSE) images, isothermal remanent magnetization (IRM) demagnetization curves from 6 to 300 K, thermomagnetic curves from 100 to 700°C, and first-order reversal curve (FORC) diagrams of representative serpentinized peridotites. The serpentinization degree increases from the bottom to top plots. Grain density, serpentinization degree, and magnetite amount are shown as *d* (g/cm^3), S (%), and *m* (wt %), respectively.

increasing degrees of serpentinization, scattered, submicron-sized magnetite-bearing veins are well developed. Detailed descriptions of petrological observations from 13 representative samples are reported in supporting information.

For measurements of rock magnetic properties and grain density, four cubic subsamples (∼2 cm cube) and several chip specimens (∼500 mg) were cut from the rock samples. The cubic subsamples were used for bulk grain density, natural remanent magnetization (NRM), and magnetic susceptibility measurements. Chip specimens were used for thermomagnetic experiments in low-temperature and high-temperature conditions, magnetic hysteresis analyses mainly for saturation magnetization measurements, and first-order reversal curve (FORC) measurements.

In order to estimate the serpentinization degree of serpentinized peridotites, bulk grain density (d) was measured on all cubic subsamples using a high precision microbalance with a resolution of 0.01 mg and a gas-pycnometer (AccuPycTM 1330 Pycnometer) at the Atmosphere and Ocean Research Institute (AORI), The University of Tokyo.

The NRM intensity was measured on all cubic subsamples by using a spinner magnetometer (Natsuhara Giken DSPIN) at the AORI. The measurements of magnetic susceptibility were conducted on all cubic subsamples using the AGICO KLY-3 Kappabridge installed at the Center for Advanced Marine Core Research (CMCR), Kochi University. Low-temperature and high-temperature magnetic analyses were performed on chip specimens for representative rock samples. The low-temperature experiment was performed using a magnetic property measurement system (MPMS, Quantum Design Inc.) installed at the CMCR. After cooling in a zero field, isothermal remanent magnetization (IRM) was imparted to the samples with an external field of 3 T at 6 K. The IRM was continuously measured every 2 K steps during the warming period up to 300 K. The MPMS was also used for measuring frequency dependency of magnetic susceptibility by varying both the operating frequency (1, 10, 100, and 1000 Hz) and temperature ranging 10–300 K. The high-temperature experiment of saturation magnetization was conducted under an inducing magnetic field of 0.5 T in a vacuum ($\sim$1 Pa) by using a magnetic balance (Natsuhara Giken MNB-89) at the CMCR. The chip specimens were heated from 50°C to 700°C and cooled back to 30°C at a rate of 12°C/min. The FORCs measurements were conducted using an alternating gradient magnetometer (AGM, Princeton Measurements Corporation MicroMag 2900) at the CMCR. The FORC diagrams provide information on the distribution of coercivity (Hc) for a magnetic grain assemblage [e.g., *Roberts et al*., 2000]. The field spacing was set to 2.25 mT, and a total of 100 FORCs were measured with Hc values between 0 and 120 mT, and a local interaction field (Hu) between -40 and 40 mT. We used a smoothing factor [*Roberts et al*., 2000] of 2. The irregularFORC software [*Zhao et al*., 2015] was used for data processing. Magnetic hysteresis parameters including saturation magnetization (Ms) was measured on several chip materials (N = 4–12) for each serpentinized peridotite by using a vibrating sample magnetometer (VSM) at the CMCR. The remanence ratio (saturation remanent magnetization to saturation magnetization) against the coercivity ratio (remanent coercivity to coercivity) were utilized to estimate the ferromagnetic grain size in rock samples based on the Day plot [e.g., *Day et al*., 1977].

4. Results

4.1. Density and Serpentinization Degree

The serpentinization degree was estimated from the bulk grain density. The density values of olivine and pyroxene are 3.37 and 3.28 g/cm^3, respectively, whereas the density of serpentine is 2.55 g/cm^3; thus, the bulk grain density should decrease after serpentinization. *Miller and Christensen* [1997] analyzed ophiolitic and abyssal serpentinized peridotites and proposed the following empirical equation between the density (d) and serpentinization degree (S): $S = (3.3 - d)/0.785$. Magnetite has a large density of 5.2 g/cm^3 and biases the degree of serpentinization. We adopted the improved equation proposed by *Oufi et al*. [2002] who considered the magnetite volume fraction (m) as follows: $S = (3.3 - [(d - 5.2 * m)/(1 - m)]/0.785$. The magnetite mass fraction of each sample was estimated from the saturation magnetization by assuming that magnetite is the only mineral contributing to saturation magnetization in samples (Ms of pure magnetite is 92 Am^2/kg). Observed Ms values were 0.1–5.0 Am^2/kg (average 2.1 Am^2/kg), which are equivalent to a magnetite amount of 0.1–5.5 wt % (average 2.3 wt %) (Figure 3a).

Grain density values ranged from 2.63 to 3.17 g/cm^3 (average 2.80 g/cm^3) (Figure 3a). The relative standard deviation (RSD) for the density of each serpentinized peridotite was less than 1% in general (Figure 4), thus indicating that density varies little within each rock sample.

The investigated 30 serpentinized peridotite samples showed large variations in the degree of serpentinization between samples, i.e., 17–100%, where the majority of samples had high degrees of serpentinization ($S > 70\%$) (Figure 3b), six samples had moderate degrees of serpentinization (S = 40–70%), and six samples had low degrees of serpentinization ($S < 40\%$).

4.2. Magnetic Properties

The NRM intensity and volume-normalized magnetic susceptibility of serpentinized peridotite were 0.2–8.4 A/m (average 2.2 A/m) and 0.002–0.087 SI (average 0.035 SI), respectively (Figures 3c and 3d). The

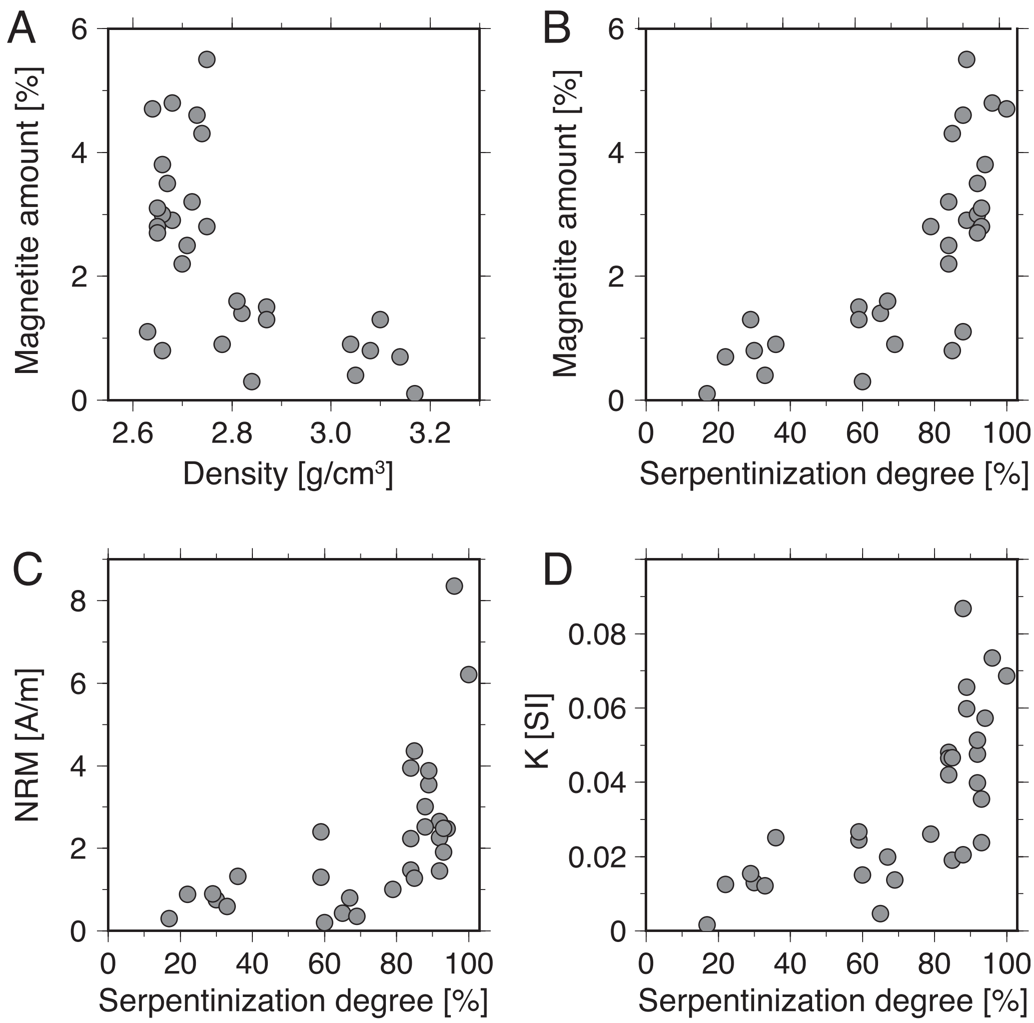

Figure 3. Relationships between (a) the grain density and magnetite amount, (b) the serpentinization degree and magnetite amount, (c) the serpentinization degree and natural remanent magnetization (NRM) intensity, and (d) the serpentinization degree and magnetic susceptibility.

Koenigsberger ratio (Q), which is the proportion of NRM to induced magnetization, was 0.4–5.7 (average 2.1) assuming an external magnetic field of 40,000 nT. More than 80% of serpentinized peridotites showed that the magnetization is dominated by remanence ($Q > 1$). Measurements of four cubic subsamples for each serpentinized peridotite indicated that the NRM and susceptibility do not vary significantly within each sample. The RSDs of NRM and susceptibility were less than 30% in the majority (>75%) of samples (Figure 4).

Thermomagnetic analyses for almost all samples showed a single high Curie temperature of ~580°C (Figure 2). The warming and cooling curves were almost identical, thus indicating that low-temperature oxidation (maghemitization) did not occur. The low-temperature measurements showed a rapid decrease of magnetization between 90 and 120 K (Figure 2), which is indicative of the Verwey transition for magnetite [e.g., *Özdemir et al.*, 1993]. These results indicate that magnetite carried the magnetization. One noteworthy feature was that the characteristic linear change of magnetization in the high-temperature thermomagnetic curve was observed in the peridotite with <20% serpentinization (6K1170-R25). This signature was likely affected by paramagnetic contribution since this sample contain low amount of magnetite (0.1 wt %).

Peridotites with high degrees of serpentinization exhibited magnetite grain aggregates within the veins (Figure 2), which had a complex growth structure with dendritic or capillary crystallization. Magnetite creation occurred in veins within olivine grains and not within pyroxene grains. Magnetite

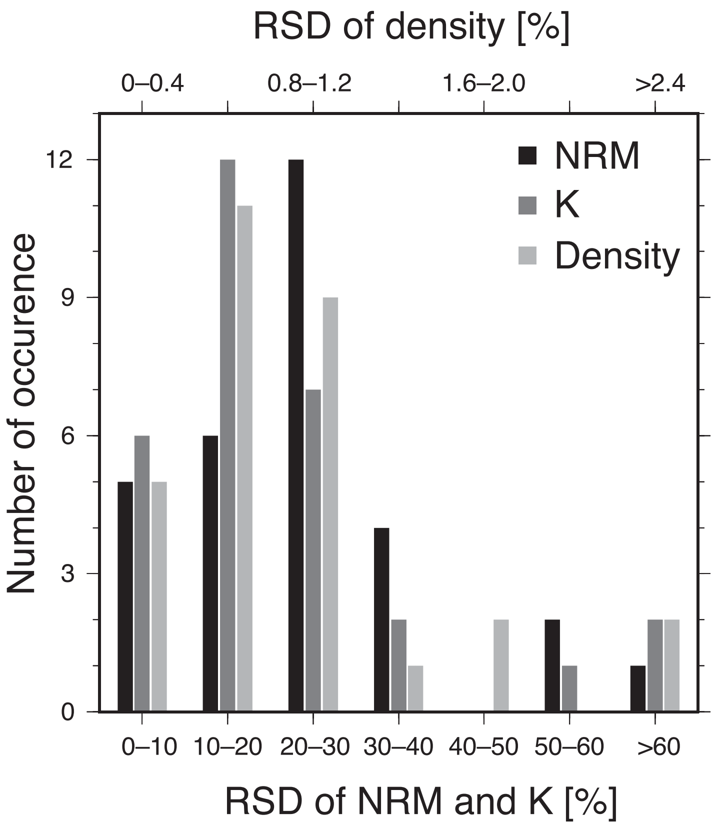

Figure 4. Relative standard deviation (RSD) of the natural remanent magnetization (NRM) intensity, magnetic susceptibility (K), and density measured on four cubic subsamples (~2 cm cube) of each of the 30 serpentinized peridotite samples.

occurred as an assemblage of needle-like grains in the highly serpentinized peridotites (Figures 5a and 5b). In contrast, in less serpentinized samples, it was developed as large, micron-sized grains along primary mineral rims or cracks (Figures 5c and 5d).

The FORC distributions for the samples with lower serpentinization degrees (<60%) showed contours diverging toward the Hu axis and coercivity (Hc) was low, i.e., ~10 mT or lower at the peak (Figure 2), which is suggestive of the dominance of multidomain (MD) grains. In contrast, FORC distributions for the samples with higher serpentinization degrees (>60%) had higher coercivities and closed contours (Figure 2), which is suggestive of a larger contribution from single-domain (SD) grains. The completely serpentinized samples showed higher coercivities and interacting fields, thus indicating the presence of elongated grains and concentration of SD grains, respectively. This signature is consistent with the microstructures on polished thin sections that showed an assemblage of needle-like grains (Figure 5b). Slightly serpentinized samples showed FORC distributions near Hc = 0 and Hu = 0, thus suggesting the presence of superparamagnetic (SP) grains (Figure 2).

The ratio of mass-normalized magnetic susceptibility to saturation magnetization (Ms) showed that only samples with serpentinization degrees of 33–60% (6K#1170R26 and DR11-002) have K/Ms value higher than upper limit of approximately 9 m/A for MD–SD magnetite grains (Figure 6a), thus supporting a greater contribution of SP grains only in slightly to moderately serpentinized peridotite [*Hunt et al.*, 1995; *Dunlop*, 1981; *Dunlop and Prévot*, 1982]. Measured in-phase susceptibility for these samples depends remarkably on frequency at low-temperature of 30 and 50 K (Figures 6b and 6c). These results suggest the presence of SP grains as well as MD grains, since a fraction of stable SD grains turn in superparamagnetic at decreased frequency [e.g., *Dearing et al.*, 1996; *Eyre*, 1997] and domain wall oscillations lag remarkably behind the driving field at low temperature [*Özdemir et al.*, 2009]. Some frequency dependence above the Verwey transition up to 300 K is likely caused by broad particle size distribution of SP grains in which in-phase susceptibilities exhibit maxima that both shift toward higher temperatures and decrease in magnitude with increasing frequency [e.g., *Worm and Jackson*, 1999]. In contrast to slightly to moderately serpentinized peridotite, frequency dependence was not clearly observed in less serpentinized sample (6K#1170R25; Figure 6d) and highly serpentinized sample (6K#1170R12; Figure 6e).

Supporting evidence for the presence of SP particles is provided by the Day plot for magnetic hysteresis parameters [e.g., *Day et al.*, 1977]. The remanence ratio (Mrs/Ms) for the samples varied between 0.08 and 0.37, and was distributed within broad area of the pseudo-single-domain (PSD) region (Figure 7). Points between the SD-MD and SP-SD mixing lines mostly have intermediate values of serpentinization degrees. These results are consistent with that some contribution of SP grains was observed in slightly to moderately serpentinized peridotites. In addition, consistent results indicating SP-like behavior are observed in the low-

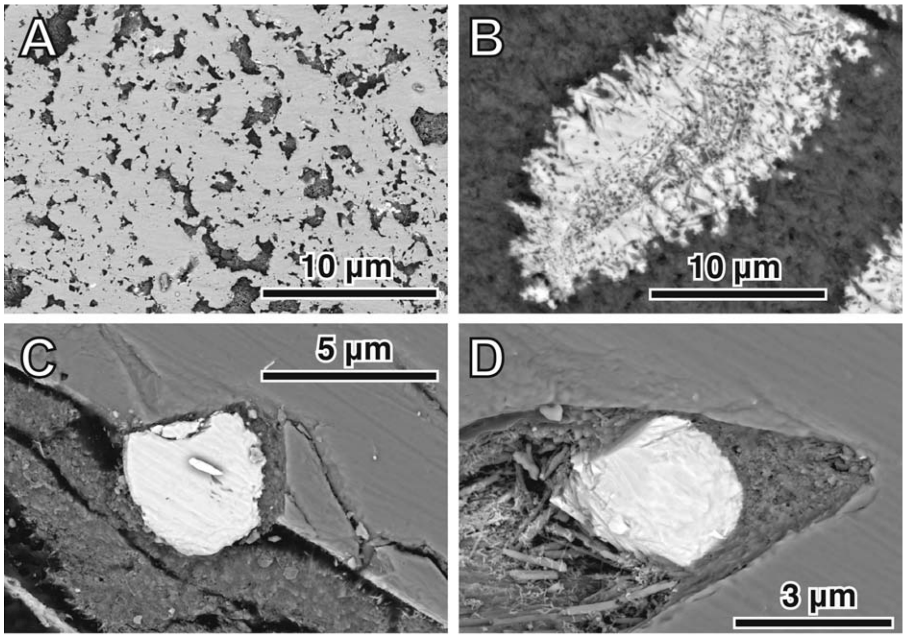

Figure 5. Back-scattered electron (BSE) images of magnetite grains showing (a) the concentration of magnetite grains in the 96% serpentinized peridotite (6K1170R12) with a magnetite amount of 4.8 wt %, (b) the assemblage of the needle-like grains in the 79% serpentinized peridotite (DR11-004) with a magnetite amount of 2.8 wt %, (c) a primary creation along the primary mineral rim in the 17% serpentinized peridotite (6K1170-R25) with a magnetite amount of 0.1 wt %, and (d) a secondary development of within cracks in the 17% serpentinized peridotite (6K1170-R25) with a magnetite amount of 0.1 wt %.

temperature SIRM curves, in which concave downward slopes at <50 K indicative of progressive thermal unblocking of SD grains were shown particularly in slightly to moderately serpentinized peridotites (Figure 2).

5. Discussion

The investigated serpentinized peridotites from the Yokoniwa Rise covered a full range of serpentinization degrees and provided a complete data set that characterizes the magnetic properties of variously altered ultramafic rocks. The presence of pure magnetite was confirmed by the high-temperature and low-temperature magnetic measurements. Magnetite grains were developed within veins, and these were created from primary minerals in the peridotites through serpentinization reaction processes. Since no magnetite grains occurred near the pyroxene grains, magnetite creation was related to the alteration of olivine. The amount of magnetite increased with the progression of serpentinization, and it was developed as an assemblage of small SD grains (Figures 5a and 5b). On the other hand, magnetite grains in slightly serpentinized peridotite were dominant in the MD state, which was possibly created through (1) a primary igneous process with olivine and pyroxene formation (Figure 5c), and/or (2) a high-temperature water rock reaction (Figure 5d). Both processes with high-temperature conditions promote the growth of magnetite grains. The former possibility is supported by oxygen fugacity in the upper mantle, in which magnetite is stable in the wustite-magnetite buffer [*Frost and McCammon*, 2008]. The latter is indicated by numerical models of chemical thermodynamics, which show that olivine is partially or entirely persistent at equilibrium and that only a small amount of magnetite should form during initial alterations at temperatures higher than 315°C [*McCollom and Bach*, 2009]. The some contribution of SP grains was observed only on slightly to moderately serpentinized, suggesting SP particle formed during the initial stages of serpentinization.

The variations of magnetite amounts, NRM intensities, and magnetic susceptibility with serpentinization degrees (Figures 3b, 3b, and 3d) are suggestive of the following features. First, the abundance of magnetite in the Yokoniwa samples appears to vary nonlinearly with serpentinization degrees. A remarkable increase of magnetite amount occurs in samples with high degrees of serpentinization (>70%), thus indicating the production of magnetite in the later stage of serpentinization processes. Second, magnetic susceptibility increases drastically with the degree of serpentinization. Third, the NRM intensity also increases with the degree of serpentinization, which is caused by the increase of magnetite production. The scatter of NRM

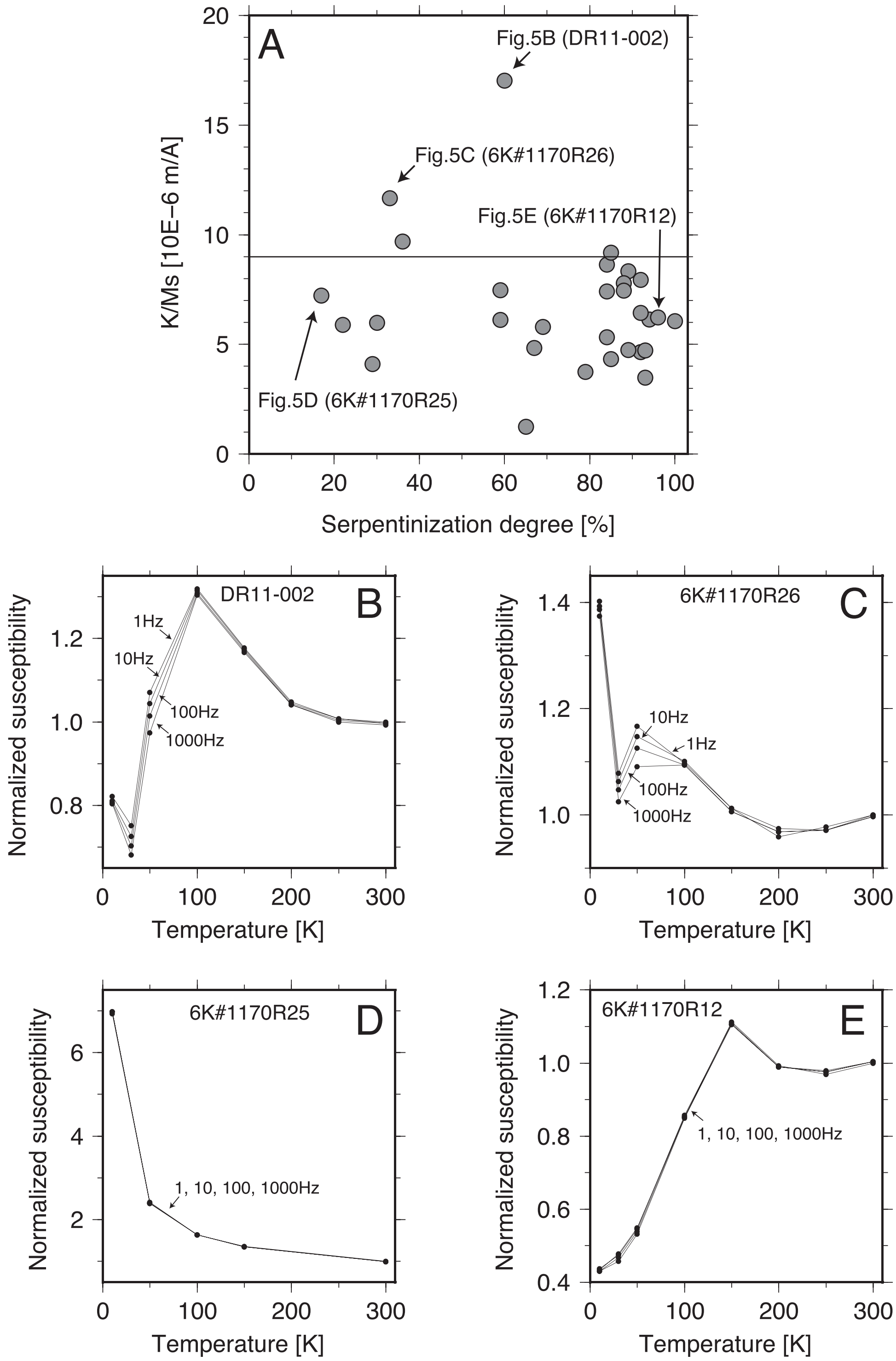

Figure 6. (a) Relationships between the serpentinization degree and the ratio of magnetic susceptibility (K) to saturation magnetization (Ms) of each sample. High K/Ms ratios in moderately serpentinized peridotite are indicative of greater superparamagnetic (SP) grain contributions. Mass-normalized K in magnetite was calculated using the density (5.2 g/cm^3) and saturation magnetization of pure magnetite (92 Am^2/kg) while assuming that the magnetic carrier of samples was pure magnetite [*Hunt et al*., 1995]. Solid line shows the upper limit of K/Ms for MD-SD magnetite grains (approximately 9 m/A) presented by *Dunlop* [1981] and *Dunlop and Prévot* [1982]. (b–e) Magnetic susceptibility and temperature curves measured at four frequencies (1, 10, 100, and 1000 Hz) for four representative samples (DR11-002, 6K#1170R26, 6K#1170R25, and 6K#1170R12). The value of measured magnetic susceptibility is normalized at by each measured value at 1 Hz and 300 K.

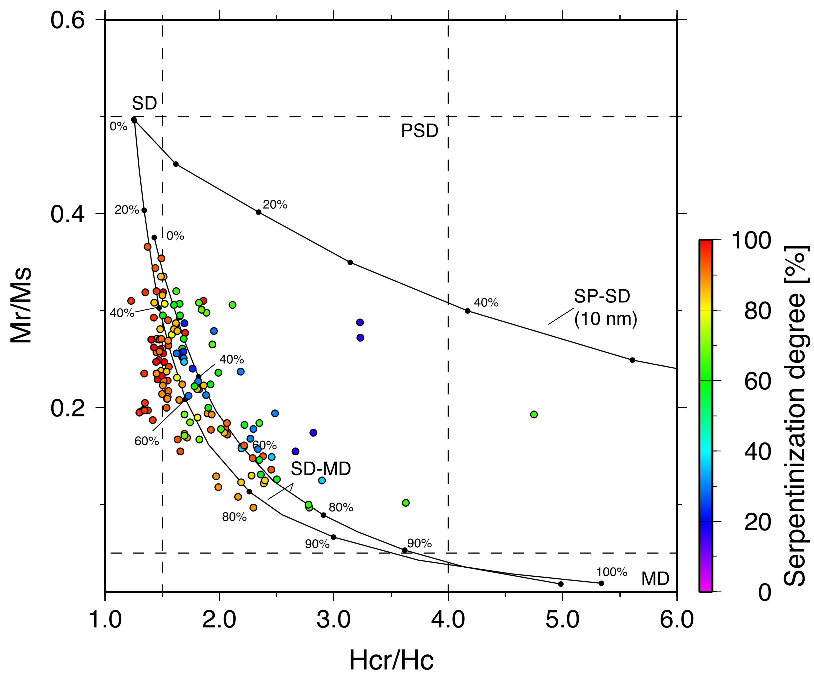

Figure 7. Day plot [e.g., *Day et al.*, 1977] for all 30 samples of serpentinized peridotites from the Yokoniwa Rise of the Central Indian Ridge. The solid lines show the theoretical mixing curves of SD-MD and SP-SD for magnetite [*Dunlop*, 2002]. SD, single-domain; MD, multidomain; SP, superparamagnetic; and PSD, pseudo-single-domain.

intensity at a particular serpentinization degree can be controlled by many factors such as the size and shape of ferromagnetic minerals and the geomagnetic field strength at the timing of remanence acquisition. The maximum value of the NRM intensity was up to 8 A/m for the rock sample with a serpentinization degree of 96%, thus indicating that the remanence as well as induced magnetization of highly serpentinized peridotite can contribute to magnetic anomalies.

A drastic increase in the amount of magnetite after the progression of 60–70% serpentinization was clearly observed in our serpentinized peridotites taken from the Yokoniwa Rise in the CIR ($<$1 Myr old). Highly serpentinized peridotites with a large amount of magnetite were also reported from the Azores platform (18–35 Myr old) and the Kane Fracture Zone ($<$1–7 Myr old) at the Mid-Atlantic Ridge and the East Pacific Rise ($<$1 Myr old) [*Oufi et al.*, 2002]. These natural samples support the nonlinear increase of magnetite through the serpentinization process. In contrast, hydrothermal experiments of natural olivine (San Carlos) [*Malvoisin et al.*, 2012] showed that magnetite amounts (calculated by saturation magnetization) increase linearly during serpentinization. The discrepancy between magnetite production of experimentally serpentinized olivine and in-situ serpentinized peridotites can be possibly explained by the changes of silica activity and oxygen fugacity. *Miyoshi et al.* [2014] investigated the changes in mineralogical textures in the Iwanaidake ultramafic body and demonstrated that silica supply from orthopyroxene alteration can be a trigger for magnetite formation. The breakdown of iron-rich serpentine and brucite in the latter stage of the reaction, as proposed by *Bach et al.* [2006], *Beard et al.* [2009], and *Frost et al.* [2013] has essentially the same role as the silica supply. Thermodynamic modeling by *Frost et al.* [2013] highlighted the importance of the redox budget and demonstrated that the transition from brucite-serpentine to brucite-serpentine-magnetite assemblages is accompanied by an increase of the oxygen fugacity (water/rock ratio) with a minor change of silica activity. Since redox conditions should be different between natural (open) experiments and laboratory experiments (closed), such as those by *Malvoisin et al.* [2012], the redox budget changes are likely the responsible factor driving the discrepancy between the linear and nonlinear changes of magnetite creation during serpentinization.

The total amount of magnetite creation during serpentinization is also controlled by various factors such as primary rock compositions and temperature. Thermodynamic equilibrium models [*Klein et al.*, 2013a] and oxygen-isotope analyses for natural samples [*Klein et al.*, 2013b] have demonstrated that serpentinized peridotite passing though the reaction at higher temperatures ($>$200°C) carries abundant magnetite with the involvement of Fe-poor brucite. Moreover, thermodynamic modeling by *Klein et al.* [2013a] predicted that pyroxenite does not produce magnetite. The Yokoniwa serpentinized peridotite of 6K1170R22 with abundant orthopyroxene showed a high degree of serpentinization (85%), but a small amount of magnetite (0.8 wt %), thus lending further credence to the role of orthopyroxene. As discussed above, orthopyroxene could play an important role in the nonlinear change of magnetite creation, however, excessive amounts of orthopyroxene control the total amount of magnetite creation. There may be other factors for magnetite formation process during serpentinization, but in any case the magnetization of serpentinized peridotite was strongly related to degree of serpentinization and was carried by magnetite grains created through serpentinization.

6. Conclusions

A rock magnetic and petrological study of 30 serpentinized peridotite samples from the Yokoniwa Rise in the Central Indian Ridge revealed the following findings. The magnetic carrier of the samples is pure magnetite, which did not suffer from low-temperature oxidation. The results from rock magnetic and petrological analyses illustrated the variation of magnetic properties of serpentinized peridotite with serpentinization degrees of 17–100%. The amount of magnetite in serpentinized peridotites increased nonlinearly up to 5.5 wt % with the serpentinization reaction progression, thus resulting in high NRM intensity ($\sim$8.4 A/m) and high magnetic susceptibility ($\sim$0.087 SI). Highly serpentinized peridotites have a well-developed serpentine mesh texture. The grain size of magnetite formed during serpentinization changes with the progression of the serpentinization reaction. The MD grains were formed through a primary igneous process and/or the initial stages of serpentinization under high-temperature conditions. The SP particles were also formed during the initial stages of serpentinization. The SD magnetite was formed during the later stage of serpentinization, and it occurs within the mesh structure as needle-like grains with strong magnetic interactions.

The investigated samples, for which detailed magnetic properties of abyssal serpentinized peridotites were characterized, represent a wide range of serpentinization degrees from a single location of the NTO massif near the spreading axes. The data set clearly demonstrates the nonlinear nature of the magnetization and provides strong constraints on the generation of magnetite during the progression of the serpentinization process in a slow-spreading ridge setting. Furthermore, it offers a useful benchmark for understanding magnetic anomalies associated with ultramafic-hosted hydrothermal systems and OCCs.

Acknowledgments
We appreciate the onboard crews of the R/Vs *Yokosuka* and *Hakuho-maru* and the support team of the submersible *SHINKAI 6500* for their support during the observation cruises by JAMSTEC. Furthermore, we are grateful to the onboard scientific parties of the YK09-13-leg2 and KH10-6 cruises for their helpful support with the data acquisition. We utilized rock samples archived in the GANSEKI database (http://www.godac.jamstec.go.jp/ganseki) managed by JAMSTEC. This study was performed under the cooperative research program of CMCR, Kochi University (accept 14A037, 14B034, 15A047, and 15B042). Lastly, we express our sincere appreciation to Y. Yamamoto and K. Kodama for his kind support with rock magnetic analyses at the CMCR, and Y. Dan, I. Yamazaki, K. Kimura, and T. Chibiki for their help with SEM observation at the Hitachi High-Tech laboratory. This study was supported by a MEXT Grant-in-Aid for Scientific Research on Innovative Areas titled "Project TAIGA; Trans-crustal advection and in situ biogeochemical process of global sub-seafloor aquifer" (20109002) from the JSPS Grants-in-Aid program for a JSPS fellow, and by the CREST program of the JST agency. The GMT software package [*Wessel and Smith*, 1998] was used to analyze the data and build the figures. We thank B. Moskowitz and J. Dyment for their constructive reviews.

References

Bach, W., H. Paulick, C. J. Garrido, B. Ildefonse, W. P. Meurer, and S. E. Humphris (2006), Unraveling the sequence of serpentinization reactions: Petrography, mineral chemistry, and petrophysics of serpentinites from MAR 15°N (ODP Leg 209, Site 1274), *Geophys. Res. Lett.*, *33*, L13306, doi:10.1029/2006GL025681.

Beard, J. S., B. R. Frost, P. Fryer, A. McCaig, R. Searle, B. Ildefonse, P. Zinin, and S. K. Sharma (2009), Onset and progression of serpentinization and magnetite formation in olivine-rich troctolite from IODP Hole U1309D, *J. Petrol.*, *50*(3), 387–403, doi:10.1093/petrology/egp004.

Briais, A. (1995), Structural analysis of the segmentation of the Central Indian Ridge between 20°30′S and 25°30′S (Rodriguez Triple Junction), *Mar. Geophys. Res.*, *17*(5), 431–467, doi:10.1007/BF01371787.

Cannat, M., et al. (1995), Thin crust, ultramafic exposures, and rugged faulting patterns at the Mid-Atlantic Ridge (22°–24°N), *Geology*, *23*(1), 49–52, doi:10.1130/0091-7613(1995)023<0049:TCUEAR>2.3.CO;2.

Day, R., M. Fuller, and V. A. Schmidt (1977), Hysteresis properties of titanomagnetites: Grain-size and compositional dependence, *Phys. Earth Planet. Inter.*, *13*(4), 260–267, doi:10.1016/0031-9201(77)90108-X.

Dearing, J. A., R. J. L. Dann, K. Hay, J. A. Lees, P. J. Loveland, B. A. Maher, and K. O'Grady (1996), Frequency-dependent susceptibility measurements of environmental materials, *Geophys. J. Int.*, *124*(1), 228–240, doi:10.1111/j.1365-246X.1996.tb06366.x.

Dick, H. J. B. (1989), Abyssal peridotites, very slow spreading ridges and ocean ridge magmatism, *Geol. Soc. Spec. Publ.*, *42*(1), 71–105, doi:10.1144/GSL.SP.1989.042.01.06.

Dunlop, D. J. (1981), The rock magnetism of fine particles, *Phys. Earth Planet. Inter.*, *26*(1), 1–26, doi:10.1016/0031-9201(81)90093-5.

Dunlop, D. J. (2002), Theory and application of the Day plot (Mrs/Ms versus Hcr/Hc), 1. Theoretical curves and tests using titanomagnetite data, *J. Geophys. Res.*, *107*(B3), doi:10.1029/2001JB000486.

Dunlop, D. J., and M. Prévot (1982), Magnetic properties and opaque mineralogy of drilled submarine intrusive rocks, *Geophys. J. Int.*, *69*(3), 763–802, doi:10.1111/j.1365-246X.1982.tb02774.x.

Dyment, J., J. Arkani-Hamed, and A. Ghods (1997), Contribution of serpentinized ultramafics to marine magnetic anomalies at slow and intermediate spreading centres: Insights from the shape of the anomalies, *Geophys. J. Int.*, *129*(3), 691–701, doi:10.1111/j.1365-246X.1997.tb04504.x.

Escartín, J., G. Hirth, and B. Evans (1997), Effects of serpentinization on the lithospheric strength and the style of normal faulting at slow-spreading ridges, *Earth Planet. Sci. Lett.*, *151*(3–4), 181–189, doi:10.1016/S0012-821X(97)81847-X.

Eyre, J. K. (1997), Frequency dependence of magnetic susceptibility for populations of single-domain grains, *Geophys. J. Int.*, *129*(1), 209–211, doi:10.1111/j.1365-246X.1997.tb00951.x.

Ferré, E. C., S. A. Friedman, F. Martín-Hernández, J. M. Feinberg, J. A. Conder, and D. A. Ionov (2013), The magnetism of mantle xenoliths and potential implications for sub-Moho magnetic sources, *Geophys. Res. Lett.*, *40*, 105–110, doi:10.1029/2012GL054100.

Fouquet, Y., et al. (2010), Geodiversity of hydrothermal processes along the Mid-Atlantic Ridge and ultramafic-hosted mineralization: A new type of oceanic Cu-Zn-Co-Au volcanogenic massive sulfide deposit, in *Diversity of Hydrothermal Systems on Slow Spreading Ocean Ridges*, vol. 188, edited by P. A. Rona, C. W. Devey, J. Dyment, B. J. Murton, pp. 321–367, AGU, Washington, D. C.

Frost, B. R., K. A. Evans, S. M. Swapp, J. S. Beard, and F. E. Mothersole (2013), The process of serpentinization in dunite from New Caledonia, *Lithos*, *178*, 24–39, doi:10.1016/j.lithos.2013.02.002.

Frost, D. J., and C. A. McCammon (2008), The redox state of Earth's mantle, *Annu. Rev. Earth Planet. Sci.*, *36*(1), 389–420, doi:10.1146/annurev.earth.36.031207.124322.

Fujii, M., K. Okino, T. Sato, H. Sato, and K. Nakamura (2016), Origin of magnetic highs at ultramafic hosted hydrothermal systems: Insights from the Yokoniwa site of Central Indian Ridge, *Earth Planet. Sci. Lett.*, *441*, 26–37, doi:10.1016/j.epsl.2016.02.018.

Honsho, C., K. Tamaki, and H. Fujimoto (1996), Three-dimensional magnetic and gravity studies of the Rodriguez Triple Junction in the Indian Ocean, *J. Geophys. Res.*, *101*(B7), 15,837–15,848, doi:10.1029/96JB00644.

Hunt, C. P., B. M. Moskowitz, and S. K. Banerjee (1995), Magnetic properties of rocks and minerals, in *Rock Physics & Phase Relations*, edited by T. J. Ahrens, pp. 189–204, AGU, Washington, D. C.

Katayama, I., K. Hirauchi, K. Michibayashi, and J. Ando (2009), Trench-parallel anisotropy produced by serpentine deformation in the hydrated mantle wedge, *Nature*, *461*(7267), 1114–1117.

Klein, F., W. Bach, and T. M. McCollom (2013a), Compositional controls on hydrogen generation during serpentinization of ultramafic rocks, *Lithos*, *178*, 55–69, doi:10.1016/j.lithos.2013.03.008.

Klein, F., W. Bach, S. E. Humphris, W.-A. Kahl, N. Jöns, B. Moskowitz, and T. S. Berquó (2013b), Magnetite in seafloor serpentinite—Some like it hot, *Geology*, *42*(2), 135–138, doi:10.1130/G35068.1.

Kumagai, H., et al. (2008), Geological background of the Kairei and Edmond hydrothermal fields along the Central Indian Ridge: Implications of their vent fluids' distinct chemistry, *Geofluids*, *8*(4), 239–251, doi:10.1111/j.1468-8123.2008.00223.x.

Maffione, M., A. Morris, O. Plümper, and D. J. J. van Hinsbergen (2014), Magnetic properties of variably serpentinized peridotites and their implication for the evolution of oceanic core complexes, *Geochem. Geophys. Geosyst.*, *15*, 923–944, doi:10.1002/2013GC004993.

Malvoisin, B., J. Carlut, and F. Brunet (2012), Serpentinization of oceanic peridotites: 1. A high-sensitivity method to monitor magnetite production in hydrothermal experiments, *J. Geophys. Res.*, *117*, B01104, doi:10.1029/2011JB008612.

McCollom, T. M., and W. Bach (2009), Thermodynamic constraints on hydrogen generation during serpentinization of ultramafic rocks, *Geochim. Cosmochim. Acta*, *73*(3), 856–875, doi:10.1016/j.gca.2008.10.032.

Mendel, V., D. Sauter, P. Patriat, and M. Munschy (2000), Relationship of the Central Indian Ridge segmentation with the evolution of the Rodrigues Triple Junction for the past 8 Myr, *J. Geophys. Res.*, *105*(B7), 16,563–16,575, doi:10.1029/2000JB900098.

Michael, P. J., et al. (2003), Magmatic and amagmatic seafloor generation at the ultraslow-spreading Gakkel ridge, Arctic Ocean, *Nature*, *423*(6943), 956–961.

Miller, D. J., and N. I. Christensen (1997), Seismic velocities of lower crustal and upper mantle rocks from the slow-spreading Mid-Atlantic Ridge, south of the Kane Fracture Transform Zone (MARK), *Proc. Ocean Drill. Program Sci. Results*, *153*, 437–454.

Miyoshi, A., T. Kogiso, N. Ishikawa, and K. Mibe (2014), Role of silica for the progress of serpentinization reactions: Constraints from successive changes in mineralogical textures of serpentinites from Iwanaidake ultramafic body, Japan, *Am. Mineral.*, *99*(5–6), 1035–1044, doi:10.2138/am.2014.4748.

Morishita, T., K. Hara, K. Nakamura, T. Sawaguchi, A. Tamura, S. Arai, K. Okino, K. Takai, and H. Kumagai (2009), Igneous, alteration and exhumation processes recorded in abyssal peridotites and related fault rocks from an oceanic core complex along the Central Indian Ridge, *J. Petrol.*, *50*(7), 1299–1325, doi:10.1093/petrology/egp025.

Morishita, T., K. Nakamura, T. Shibuya, H. Kumagai, T. Sato, K. Okino, H. Sato, R. Nauchi, K. Hara, and R. Takamaru (2015), Petrology of peridotites and related gabbroic rocks around the Kairei Hydrothermal Field in the Central Indian Ridge, in *Subseafloor Biosphere Linked to Hydrothermal Systems*, edited by J. Ishibashi, K. Okino, and M. Sunamura, pp. 177–193, Springer, Japan.

Munschy, M., and R. Schlich (1989), The Rodriguez Triple Junction (Indian Ocean): Structure and evolution for the past one million years, *Mar. Geophys. Res.*, *11*(1), 1–14, doi:10.1007/BF00286244.

Nakamura, K., T. Morishita, W. Bach, F. Klein, K. Hara, K. Okino, K. Takai, and H. Kumagai (2009), Serpentinized troctolites exposed near the Kairei Hydrothermal Field, Central Indian Ridge: Insights into the origin of the Kairei hydrothermal fluid supporting a unique microbial ecosystem, *Earth Planet. Sci. Lett.*, *280*(1–4), 128–136, doi:10.1016/j.epsl.2009.01.024.

Okino, K., K. Matsuda, D. M. Christie, Y. Nogi, and K. Koizumi (2004), Development of oceanic detachment and asymmetric spreading at the Australian-Antarctic Discordance, *Geochem. Geophys. Geosyst.*, *5*, Q12012, doi:10.1029/2004GC000793.

Okino, K., K. Nakamura, and H. Sato (2015), Tectonic background of four hydrothermal fields along the Central Indian Ridge, in *Subseafloor Biosphere Linked to Hydrothermal Systems*, edited by J. Ishibashi, K. Okino, and M. Sunamura, pp. 133–146, Springer, Japan.

Oufi, O., M. Cannat, and H. Horen (2002), Magnetic properties of variably serpentinized abyssal peridotites, *J. Geophys. Res.*, *107*(B5), doi:10.1029/2001JB000549.

Özdemir, Ö., D. J. Dunlop, and B. M. Moskowitz (1993), The effect of oxidation on the Verwey transition in magnetite, *Geophys. Res. Lett.*, *20*(16), 1671–1674, doi:10.1029/93GL01483.

Özdemir, Ö., D. J. Dunlop, and M. Jackson (2009), Frequency and field dependent susceptibility of magnetite at low temperature, *Earth Planets Space*, *61*(1), 125–131, doi:10.1186/BF03352892.

Roberts, A. P., C. R. Pike, and K. L. Verosub (2000), First-order reversal curve diagrams: A new tool for characterizing the magnetic properties of natural samples, *J. Geophys. Res.*, *105*(B12), 28,461–28,475, doi:10.1029/2000JB900326.

Sato, T., K. Okino, and H. Kumagai (2009), Magnetic structure of an oceanic core complex at the southernmost Central Indian Ridge: Analysis of shipboard and deep-sea three-component magnetometer data, *Geochem. Geophys. Geosyst.*, *10*, Q06003, doi:10.1029/2008GC002267.

Szitkar, F., J. Dyment, Y. Fouquet, C. Honsho, and H. Horen (2014), The magnetic signature of ultramafic-hosted hydrothermal sites, *Geology*, *42*(8), 715–718, doi:10.1130/G35729.1.

Takai, K., K. Nakamura, K. Suzuki, F. Inagaki, K. H. Nealson, and H. Kumagai (2006), Ultramafics-Hydrothermalism-Hydrogenesis-HyperSLiME (UltraH3) linkage: A key insight into early microbial ecosystem in the Archean deep-sea hydrothermal systems, *Paleontol. Res.*, *10*(4), 269–282, doi:10.2517/prpsj.10.269.

Toft, P. B., J. Arkani-Hamed, and S. E. Haggerty (1990), The effects of serpentinization on density and magnetic susceptibility: A petrophysical model, *Phys. Earth Planet. Inter.*, *65*(1–2), 137–157, doi:10.1016/0031-9201(90)90082-9.

Wessel, P., and W. H. F. Smith (1998), New, improved version of generic mapping tools released, *Eos Trans., AGU*, *79*(47), 579, doi:10.1029/98EO00426.

Worm, H.-U., and M. Jackson (1999), The superparamagnetism of Yucca Mountain Tuff, *J. Geophys. Res.*, *104*(B11), 25,415–25,425, doi:10.1029/1999JB900285.

Zhao, X., D. Heslop, and A. P. Roberts (2015), A protocol for variable-resolution first-order reversal curve measurements, *Geochem. Geophys. Geosyst.*, *16*(5), 1364–1377, doi:10.1002/2014GC005680.